ACS APPLIED ENERGY MATERIALS

Open Access

This article is licensed under CC-BY 4.0

www.acsaem.org

Article

In Situ Investigation of HfO_x Atomic Layer Deposition on $(Ag,Cu)(In,Ga)Se_2$ Thin-Film Solar Cell Absorbers: Role of Absorber Bulk Composition and Surface Treatment in HfO_x Growth

Melike Babucci,* Lars Stolt, Esko Kokkonen, Rainer Timm, Joachim Schnadt, Charlotte Platzer-Björkman, Tobias Törndahl, and Natalia M. Martin*

Cite This: *ACS Appl. Energy Mater.* 2026, 9, 886−895

Read Online

ACCESS | Metrics & More | Article Recommendations | Supporting Information

ABSTRACT: Atomic layer deposition (ALD) of HfO_x layers has emerged as a promising strategy for interface passivation in chalcopyrite-based thin-film solar cells. However, the nucleation dynamics of $(Ag,Cu)(In,Ga)Se_2$ (ACIGS) absorbers remain insufficiently understood, particularly regarding the interplay between absorber composition and alkali postdeposition treatments (PDTs). Here, we employ *in situ* ambient pressure X-ray photoelectron spectroscopy (AP-XPS) to investigate the initial surface chemistry during HfO_x ALD on ACIGS thin-film solar cell absorbers with high [Ga]/([Ga]+[In]) (GGI) ratio subjected to RbF-PDT and compare the findings with low-GGI counterparts (Martin et al., *ACS Appl. Energy Mater.* **2025**, *8*, 461−472). The results show that high-GGI ACIGS surfaces are strongly Cu-depleted and enriched in Se and alkali-metal-containing secondary phases, which hinders tetrakisdimethylamido-hafnium (TDMA-Hf) precursor adsorption and delays oxide nucleation, in contrast to low-GGI ACIGS that allow quicker and more efficient HfO_x growth. Water pulses are identified as essential for reactivating the RbF-treated high-GGI surface by generating hydroxyl groups, thereby enabling metal precursor activation. The distinct formation of Ga−F and In−O species is only observed on high-GGI ACIGS together with increased Na diffusion, reflecting different surface chemistry for a higher Ga content of ACIGS as compared to the low Ga case. These findings demonstrate that bulk composition and alkali-PDT strongly influence ALD reactivity, surface passivation, and interface formation, with direct implications for composition-specific optimization of ACIGS solar cells.

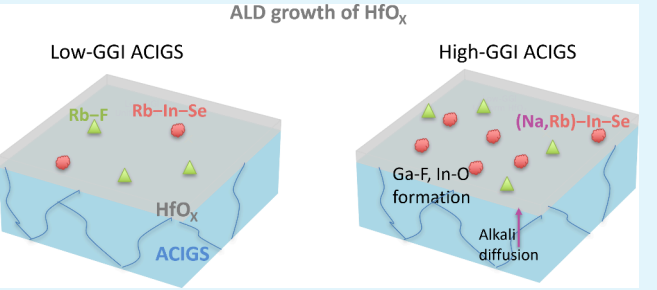

KEYWORDS: *thin-film solar cells, ACIGS, alkali-PDT, AP-XPS, HfO_x, ALD*

Downloaded via UPPSALA UNIV on March 31, 2026 at 10:40:41 (UTC).
See https://pubs.acs.org/sharingguidelines for options on how to legitimately share published articles.

1. INTRODUCTION

$Cu(In,Ga)Se_2$ (CIGS) thin-film solar cells have long been recognized for their high and stable efficiencies in both laboratory-scale devices and commercial modules. However, bridging the gap to the theoretical efficiency limit of 30% remains a challenge. A key compositional parameter in CIGS absorbers is the [Ga]/([Ga]+[In]) ratio (GGI), which directly affects the band gap energy and thus the device performance. An increased GGI ratio shifts the band gap from ∼1.0 eV (pure $CuInSe_2$) to ∼1.7 eV (pure $CuGaSe_2$), enabling better voltage output and facilitating band gap grading. A promising strategy for further performance enhancement is the incorporation of silver into the absorber layer,[1] forming $(Ag,Cu)(In,Ga)Se_2$ (ACIGS), which has been shown to improve grain growth, reduce defect densities, and modify electronic properties in favor of higher open-circuit voltage and fill factor. This modification has recently enabled record-breaking efficiencies, such as the 23.64% achieved by Keller et al.[2] In parallel, postdeposition treatments (PDTs) with alkali metal fluorides—typically KF, RbF, or CsF—have become standard for enhancing CIGS and ACIGS device performance.[3−5] These treatments, also used in the current record-holding devices, are known to induce beneficial changes near the absorber surface and at interfaces.[6] Though the precise mechanisms, especially those involving Ag and alkali elements, are still under investigation, evidence increasingly points to key effects at grain boundaries and the heterojunction interface, including redistribution of elements and changes in interface chemistry. Given this critical role of interfaces in device performance, strategies that can modulate or stabilize these regions are of growing interest.

The interfaces surrounding the absorber—both the front, which faces the incident light, and the back—play a critical role

Received: October 3, 2025
Revised: January 5, 2026
Accepted: January 6, 2026
Published: January 12, 2026

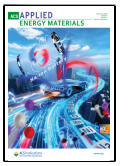

© 2026 The Authors. Published by American Chemical Society

in solar cell performance, with the junction between the p-type absorber and the n-type buffer layer being especially important. Characteristics such as band alignment, surface band gap modification, interface defect density, and alkali element distribution are critical to charge carrier dynamics. In efforts to improve these characteristics, ultrathin HfO_x layers deposited by atomic layer deposition (ALD) have emerged as effective passivation barriers in conventional CIGS structures, helping suppress recombination at both front and rear interfaces.[7,8] It is expected that surface passivation can reduce interface recombination by eliminating some defects. The HfO_2 has a high bandgap (>5 eV) and will create a large positive conduction band offset (CBO) relative to ACIGS, which can effectively block electrons if the layer is fully covering and a few nanometers thick.

Understanding the surface reactions that occur during the initial ALD cycles is essential for engineering improved interfaces with ALD layers. Previous studies[9,10] on HfO_2 growth on semiconductors such as InAs suggest a "self-cleaning" effect during the early stages of ALD, where precursor adsorption plays a critical role in determining interface quality. Drawing inspiration from this, our recent study[11] suggests that the ACIGS surface actively participates in ALD by supplying oxygen for HfO_x formation during the first metal precursor half-cycle, whereas RbF treatment appears to delay growth by reducing available adsorption sites and limiting oxygen diffusion. However, the growth behavior of ALD passivation layers as a function of absorber surface treatments and bulk compositions remains not fully understood.

In the previous study,[11] we employed ambient pressure X-ray photoelectron spectroscopy (AP-XPS) to investigate the initial surface chemistry *in situ* during the first ALD cycle of HfO_x on low-GGI ACIGS with and without a RbF PDT. The ability of AP-XPS to analyze surface chemistry in real time under conditions close to commercial ALD environments makes it an invaluable technique for understanding and optimizing surface reactions, film growth mechanisms, and material properties during *in situ* ALD processes.[10] The results demonstrate that dissociative adsorption of the Hf precursor, tetrakis(dimethylamido)hafnium (TDMA-Hf), occurs during the precursor pulses, with TDMA-Hf binding to surface oxygen and hydroxyl species, leading to the formation of HfO_x even during the initial exposure. We confirmed that a RbF treatment suppressed surface reactivity by reducing the available reaction sites for the TDMA-Hf precursor due to Rb and F diffusion and lower initial oxide content. Building on these findings, the present work shifts focus to a high-GGI ACIGS with a RbF-PDT, where both the wider band gap and the altered surface properties are expected to affect ALD nucleation behavior and interfacial properties. Using *in situ* AP-XPS, we monitor real-time surface reactions on high-GGI ACIGS during sequential exposures to TDMA-Hf and H_2O precursors. By comparing RbF-treated ACIGS samples with varying compositions (low- and high-GGI), we investigate how bulk composition and surface treatment influence precursor adsorption and nucleation and, consequently, ALD growth behavior.

2. EXPERIMENTAL SECTION

The sample preparation and *in situ* characterization have been described in detail in our previous study[11] and are briefly summarized below.

2.1. Sample Preparation

The ACIGS sample was fabricated on a multilayer stack of soda-lime glass (SLG)/molybdenum (Mo)/NaF/ACIGS. Molybdenum back contact was deposited on cleaned SLG substrates using DC magnetron sputtering in a commercial large-area system. The coated substrates were then cut into 500 × 500 mm^2 sections for subsequent processing steps. A NaF layer (~10 nm) was thermally evaporated onto the Mo surface before the ACIGS absorber layer was deposited. The ACIGS films were grown by coevaporation in a dedicated chamber equipped with quadrupole mass spectrometry and feedback control to precisely regulate the elemental fluxes. A modified three-stage process was employed, beginning and ending with Cu-poor conditions and incorporating a Cu-rich intermediate phase. Additionally, the absorbers exhibit a Ga gradient from back to front. The substrate temperature during deposition reached a maximum of approximately 530 °C. Following deposition, the sample was subjected to an RbF PDT. This was carried out by thermal evaporation at ~350 °C, with the deposition rate and film thickness monitored using a quartz crystal microbalance. Compositional analysis of the resulting films was conducted using X-ray fluorescence (XRF), and the elemental ratios and absorber thicknesses are detailed in Table 1. The main difference between the samples is the GGI ratio

Table 1. Bulk Compositions of RbF-Treated ACIGS Determined by XRF

sample	[Ga]/([Ga]+[In])	([Ag]+[Cu])/([Ga]+[In])	[Ag]/([Ag]+[Cu])	thickness (μm)
High-GGI ACIGS	0.82	0.92	0.51	2.2
Low-GGI ACIGS [published][11]	0.40	0.93	0.20	2.0

(0.82 vs 0.40); hence, they are hereafter referred to as high- and low-GGI, respectively. Note also the higher Ag bulk content in the high-GGI sample, with [Ag]/([Ag]+[Cu]) = 0.51, compared to the low-GGI sample.

To minimize contamination during transport for *in situ* measurements at the beamline, the as-deposited samples were sealed under a N_2 atmosphere. Prior to XPS analysis, the samples underwent a brief water rinse cleaning. At the beamline, the samples were briefly exposed to air while mounted on the sample holder, rinsed with water, and then transferred into the ultrahigh vacuum system. The total exposure time to ambient atmosphere was less than 15 min, which is comparable to the exposure duration during the fabrication process of ACIGS devices in our laboratory.

2.2. *In Situ* Characterization by AP-XPS

AP-XPS measurements were performed at the SPECIES beamline of MAX IV Laboratory (Lund, Sweden) using a dedicated ALD cell coupled to a SPECS Phoibos 150 NAP spectrometer. The cell enabled measurements at ~1.2 mbar under a continuous Ar flow (0.45 sccm) and sample temperature of 180 °C, monitored by a K-type thermocouple. TDMA-Hf and H_2O (cleaned via freeze−pump−thaw) precursors were introduced using short (0.05 s) pulses through heated lines to prevent condensation. The pulses were manually adjusted based on the surface response. Both the pulse duration and the interval between pulses were varied, and sequential pulses of the same precursor were applied. One HfO_x ALD cycle consisted of several TDMA-Hf pulses and one H_2O pulse. After several trials, the TDMA-Hf pulse duration was increased to 0.5 s due to insufficient precursor adsorption on the ACIGS surface. Samples were analyzed as-prepared, without in-vacuum treatment.

Core-level measurements were performed in swept mode using various photon energies: 1300 eV for Cu 2p, Ga 2p, F 1s, and Na 1s; 650 eV for In 3d, In 4d, Ga 3d, Se 3d, Ag 3d, Hf 4f, N 1s, C 1s, and O 1s; and 250 eV for Rb 3d. Measurements were conducted before and after selected precursor pulses (TDMA-Hf or H_2O) or ALD cycles under an argon flow and a sample temperature of 180 °C.

https://doi.org/10.1021/acsaem.5c03123
ACS Appl. Energy Mater. 2026, 9, 886−895

Additionally, selected core levels were acquired sequentially in snapshot (time-resolved) mode at 650 eV photon energy with a 3.15 s repetition rate. The analyzer slit width was set to 3 mm, and the pass energy was 50 or 100 eV, yielding energy resolutions of 0.5 and 1 eV, respectively, depending on the measurement mode (swept vs snapshot). To mitigate beam-induced damage, the sample was raster-scanned during acquisition. The resulting intensity variations were negligible for relative intensity analyses. Spectra were fitted using Voigt profiles and linear backgrounds, with appropriate constraints on doublet peak parameters, including spin−orbit splitting and intensity ratios for 4f, 4d, and 3d core levels. The binding energy scale was calibrated using the Se $3d_{5/2}$ peak at 54.2 eV, in agreement with values reported for similar materials. This calibration yielded consistent results across other core levels, as also observed in our recent study[11] on HfO_x deposition on low-GGI ACIGS. Relative composition was determined similar to our previous publication[11] by normalizing the peak intensities to the subshell photoionization cross sections[12] and corresponding inelastic mean free paths.[13,14] Image plot analysis was performed using the *Image Profile* project in Igor Pro.[15]

3. RESULTS AND DISCUSSION

3.1. Pre-ALD

Figure 1 and Figure S1 in the SI show the X-ray photoelectron (XP) spectra collected in an Ar atmosphere at 180 °C before and during the ALD of HfO_x on high-GGI ACIGS (GGI = 0.82). Fitting parameters identical to those used for the low-GGI ACIGS sample[11] (GGI = 0.40) in previous analyses were employed in this study. The binding energies of the analyzed core levels are listed in Table S1 in the SI.

As expected, the pre-ALD spectra (bottom panels) display characteristic signals from the ACIGS absorber, corresponding to Me−Se chalcopyrite bonds, along with Rb-related features from the RbF PDT. In addition to absorber signals indicating metal (Me)−Se bonds in the chalcopyrite structure, surface contamination by oxygen and carbon is evident, a common occurrence due to air exposure during sample preparation and handling. A single C 1s peak (gray − C I) at 284.6 eV is observed, consistent with previously reported carbon contamination on ACIGS surfaces. The O 1s spectrum consists of two distinct components: a main peak at 530.7 eV (gray − O I), attributed to metal−oxygen (Me−O) bonds, and a higher binding energy (+1.5 eV) shoulder (blue − O II), associated with hydroxyl groups (Me−OH). While signals above 532 eV could indicate organic C−O species, the lack of matching C 1s peaks around 286 eV supports their assignment to hydroxyls in this case. The In 3d and Ga 2p core levels show single-component peaks assigned to In and Ga in ACIGS (mainly Me−Se bonds). Although surface oxides like In_2O_3 and Ga_2O_3 may form after RbF treatment[16] or air exposure, often appearing as asymmetric peaks, no clear asymmetry is seen here. However, minor oxide contributions to the main peaks cannot be excluded given the energy resolution of 0.5 eV.

For the Se 3d core level, a single doublet is typically observed in ACIGS, corresponding to Se−metal (Me−Se) bonds within the chalcopyrite structure. However, for our as-prepared high-GGI ACIGS sample with RbF PDT, a broadening of the signal is observed as compared to the low-GGI ACIGS[11] and was fitted with two components indicating two different chemical environments. Note that identical fitting parameters were employed when fitting the low- and high-GGI ACIGS samples. A comparison of the Se signals in high- and low-GGI ACIGS samples is presented in Figure S2 in the SI. The Se I component at higher binding energy was used to calibrate the binding energy scale for all core levels. This

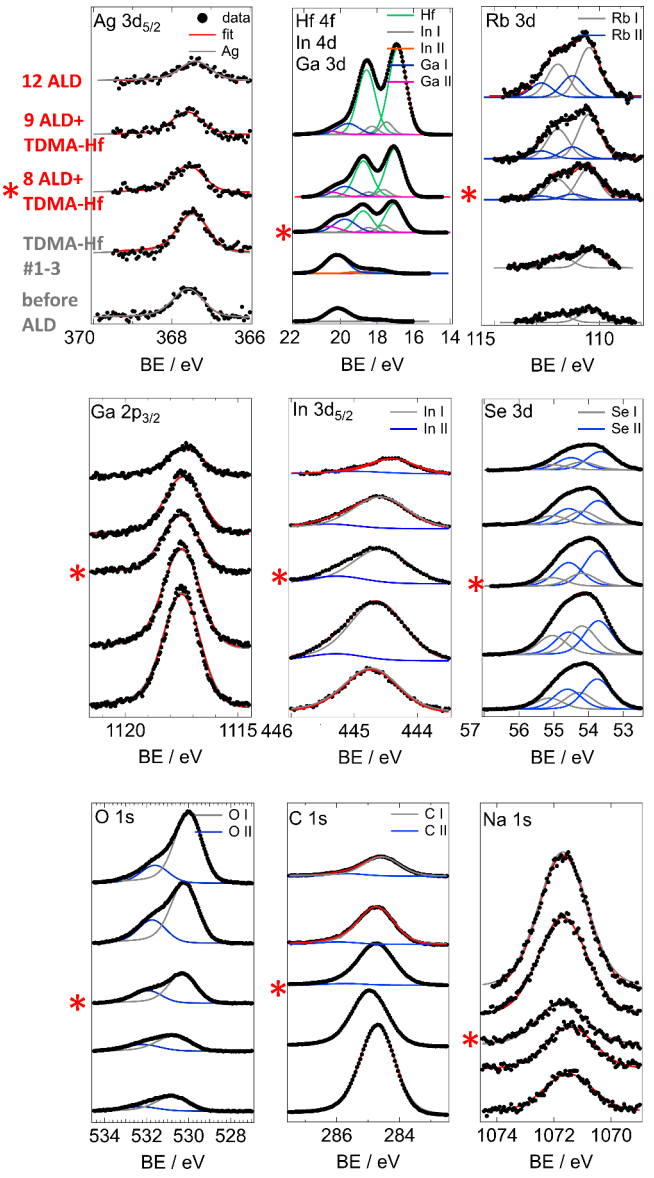

Figure 1. AP-XPS core level spectra recorded at 1300 eV (Ga 2p and Na 1s) and 650 eV (In $3d_{5/2}$, In 4d, Ga 3d, Se 3d, Hf 4f, Rb 3d, C 1s, O 1s), from the high-GGI ACIGS absorber acquired in Ar at a sample temperature of 180 °C before ALD (bottom), after three half-cycles (TDMA-Hf pulses), after several TDMA-Hf pulses following 8 ALD cycles and one extended TDMA-Hf pulse (the start of the extended pulse is denoted in each core level in the figure by a red *), after 9 ALD cycles and one extended TDMA-Hf pulse, and after 12 ALD cycles (top). One ALD cycle consisted of several TDMA-Hf pulses followed by 1 H_2O pulse. Note that the H_2O pulses were always 0.05 s, whereas TDMA-Hf pulses were increased from 0.05 to 0.5 s (extended) after 8 ALD cycles.

approach yielded binding energy values for the other core levels (Table S1) that were consistent with those reported in our previous work[11] on low-GGI ACIGS. Thus, the doublet at 54.2 eV (gray − Se I) is assigned to Se−Me bonding in ACIGS, while the secondary doublet (blue − Se II), shifted by −0.5 eV toward lower binding energy, indicates the presence of an alternative Se bonding environment distinct from that of the ACIGS phase, likely corresponding to the Rb−In−Se phase, as previously observed for the low-GGI ACIGS and also supported by the relative composition analysis presented

https://doi.org/10.1021/acsaem.5c03123
ACS Appl. Energy Mater. 2026, 9, 886−895

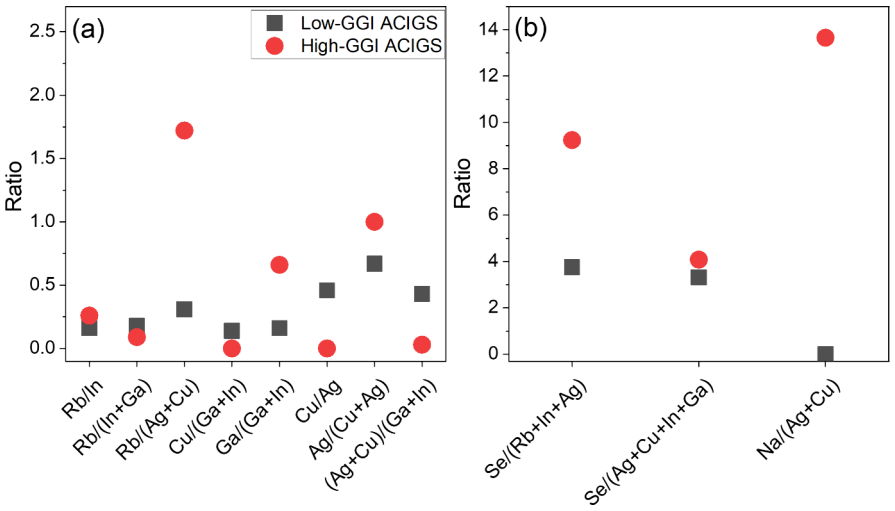

Figure 2. Relative surface composition analysis (ratios) for the low-GGI (black square) and high-GGI ACIGS (red circle) prior to ALD obtained from the XPS measurements. Note that the error bars are within the symbol size, thus may not be visible in the plot.

below, which shows an enriched In surface, despite the high GGI value in the bulk. A broadening of the Se peak due to surface defects is not excluded.

Rb species are detected in the Rb 3d core level spectrum of the ACIGS sample, which can be fitted with a single doublet (gray − Rb I) at 110.4 eV, which matches reported values for Rb−In−Se compounds (~110.0 eV), and is thus tentatively assigned here to Rb−In−Se. Given the reduced energy resolution in the present study and lack of supporting characterization, more detailed studies are needed to fully confirm this assignment. Unlike RbF compounds, which can be largely removed by rinsing, Rb−In−Se compounds are known to remain on the surface even after ammonia or water treatment.[17] The absence of new In−Se contributions in the In 3d and In 4d core levels indicates that the Se environment around In remains unchanged, with no evidence of new In−Se bonding in either the ACIGS or Rb−In−Se phases. Further, a one-to-one exchange of Rb with Cu at the surface of Cu-depleted ACIGS cannot be excluded.[18] The combination of higher Ag content and Cu depletion at the surface may point to cation exchange processes, such as the substitution of Cu by Ag and/or Rb, potentially promoting the formation of secondary phases. It is also possible that a (Ag,Rb)−In−Se phase forms, as previously reported for KF-treated (Ag,Cu)-(In,Ga)Se_2, where the formation of (Ag,K)$InSe_2$ was observed.[5] A negligible fluorine signal in the F 1s core level spectrum further indicates that most of the RbF species on the ACIGS surface have been washed during the water rinse treatment applied before the XPS measurements.

The spectra also indicate the presence of Na on the high-GGI ACIGS surface, possibly due to diffusion from the soda-lime glass substrate during annealing or Na redistribution facilitated by the RbF postdeposition treatment. The accumulation of Na is further evidenced by the Na/(Ag+Cu) surface ratio, which is significantly high (Figure 2). The incorporation of Na at the surface may influence the formation and stability of secondary phases in high-GGI ACIGS sample. This result is different for the low-GGI (0.40) ACIGS sample where a significantly lower Na signal is detected at the surface and is attributed to the higher Cu content in the case of low-GGI composition. Na tends to accumulate in Cu-deficient environments as is the case for the high-GGI ACIGS in this case, while the Cu-richer composition of low-GGI ACIGS likely limits Na retention at the surface.

A relative composition analysis of the low- and high-GGI ACIGS sample surfaces prior to ALD was obtained from the XPS measurements, and the results are summarized in Figure 2. A comparison between the bulk composition of ACIGS measured by XRF and the surface composition determined from XPS reveals significant differences near the surface prior to ALD. Both low- and high-GGI samples exhibit surfaces that are Cu- and Ga-deficient but In- and Ag-enriched relative to the bulk, consistent with earlier reports for alkali PDT of both CIGS[19] and ACIGS.[20] The measurements show also that there is almost no Cu present at the surface for the high-GGI sample (in contrast to the low-GGI sample), while still a considerable Ga amount is present, even though in lower concentration than the bulk material. The observed higher Se/(Ag+Cu+In+Ga) ratio (Figure 2) at the surface of the high-GGI sample compared to the low-GGI sample could be related to Cu depletion, which promotes Se accumulation at the surface. Further, both samples indicate increased Ag content at the surface compared to the bulk (much more pronounced for the low GGI sample), indicating the Ag dominance over Cu at the surface for both samples.

The Rb incorporation behavior in ACIGS absorbers with different GGI ratios was further assessed by comparing the Rb/(Ag+Cu) and Rb/In surface ratios (Figure 2), which revealed increased values for the high-GGI sample, indicating a higher incorporation of Rb relative to In and Cu/Ag. This points toward enhanced Rb accumulation at the surface under Ga-rich conditions. Further, significant Na is observed at the surface of the high-GGI sample, in contrast to the low GGI sample. Such behavior suggests that Ga-rich compositions may promote Rb retention and Na diffusion near the surface, potentially through altered cation distribution and defect formation.

The observed increase in Rb content may suggest the formation of Rb-containing surface phases, such as $RbInSe_2$, particularly in conjunction with Se and In enrichment and Cu depletion, but further confirmatory studies are necessary to substantiate these conclusions. This interpretation aligns with previous findings indicating that alkali metal behavior in chalcopyrite absorbers is highly sensitive to the absorber

https://doi.org/10.1021/acsaem.5c03123
ACS Appl. Energy Mater. 2026, 9, 886−895

composition. For example, Keller at al.[21] reported on the presence of a Rb−In−Se phase at the surface of Cu free high band gap Ag(In,Ga)Se_2 after RbF-PDT. Further, Maticiuc et al.[22] reported that the formation of $RbInSe_2$ is composition-dependent, with a thicker $RbInSe_2$ layer observed on Cu-depleted CIGSe absorbers, a trend that may also be relevant in the current study.

In summary, the results indicate that prior to ALD, the high-GGI ACIGS surface is Cu depleted and likely covered by some alkali-metal-containing secondary phase such as Alk(Rb,Na)-(Se,O)-metal.

3.2. Time Evolution of the HfO_x Surface Chemistry on ACIGS + RbF-PDT by AP-XPS

To monitor the surface reactions step by step, short TDMA-Hf precursor pulses (initially with a time duration of 0.05 s, which was extended to 0.5 s at a later stage as explained below) were applied sequentially to track any changes in the surface chemistry during the ALD growth. To investigate the stages of TDMA-Hf surface chemistry during HfO_x formation, we tracked the time evolution of selected core-level spectra during the ALD cycles on high-GGI ACIGS sample, focusing on changes in relative intensities and binding energies associated with both the absorber surface and the ALD precursors. Figure 3a−d presents selected image plots during the time evolution of the Rb 3d, C 1s, Ga 3d/In 4d/Hf 4f, and O 1s core levels during HfO_x growth on the ACIGS surface, while the full time-resolved growth with additional core levels is presented in Figure S3 of the SI. We note that following several trials (three TDMA-Hf pulses, followed by 8 ALD cycles (each cycle consisting of one or more TDMA-Hf pulse(s) and one H_2O pulse)), the TDMA-Hf pulse length was increased from 0.05 to 0.5 s to compensate for the limited precursor adsorption on the ACIGS surface (in contrast to the low-GGI ACIGS where a pulse length of 0.05 s was always employed). Following each pulse, time-resolved spectra were acquired over an extended period to capture the full evolution of surface species.

The time-resolved AP-XPS data show that during the initial TDMA-Hf pulses (of 0.05 s indicated by red dotted lines), no notable Hf signal (at lower binding energy superimposed in the Ga 3d/In 4d at higher binding energy in Figure 3 (d)) could be observed, reflecting slow nucleation on the high-GGI RbF-treated ACIGS surface. Thus, even though initially identical pulses were applied as in the case of the low-GGI ACIGS,[11] the HfO_x growth is much slower for the high-GGI ACIGS. The main change observed directly after the first TDMA-Hf pulse is an increase in the In 3d, Ga 3d/In 4d and O 1s signals indicating surface diffusion. In an effort to saturate the surface with the metal precursor and initiate the HfO_x growth, three subsequent TDMA-Hf pulses together with several ALD cycles are applied as indicated by the horizontal dotted lines, however without a clear change in the time-resolved spectra. Increasing the TDMA-Hf pulse duration resulted in a clear change in the time-resolved data, with a visible increase in the Hf 4f signal accompanied by a decrease in the absorber substrate signals, indicating HfO_x growth. The results indicate that a much longer metal precursor pulse and several ALD cycles/H_2O pulses are needed to initiate the ALD growth on the high-GGI ACIGS compared to low-GGI ACIGS. In an attempt to grow a thicker HfO_x layer, several H_2O (0.05 s) and TDMA-Hf (0.5 s) pulses were applied as denoted by the horizontal dotted lines (H_2O: black, TDMA-Hf: red). Some further decrease of the substrate signals and increase of the Hf signal and Me−OH

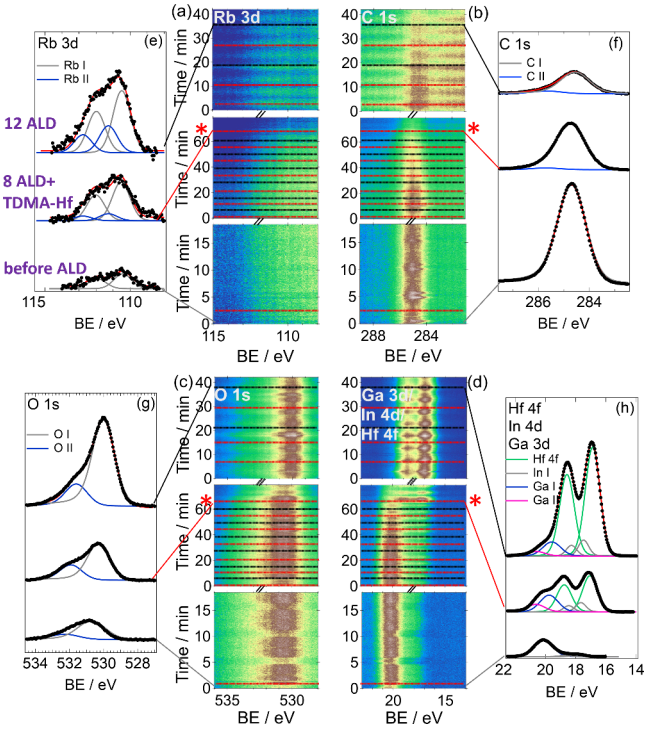

Figure 3. (a−d) *In situ* time-resolved AP-XPS measurements (snapshot mode) of the Rb 3d, C 1s, O 1s, and Ga 3d/In 4d/Hf 4f core levels during the TDMA-Hf and H_2O exposures on the RbF-treated high-GGI ACIGS surface. The timing of the TDMA-Hf pulses is marked by horizontal red lines. Panels (e−h) display AP-XP spectra recorded at 650 eV (swept mode) in Ar at 180 °C before ALD (bottom), after 8 ALD cycles + one extended TDMA-Hf pulse (middle), and after 12 ALD cycles (top). One ALD cycle consisted of several TDMA-Hf pulses followed by 1 H_2O pulse. Note that the H_2O pulses (black lines) were always 0.05 s, whereas TDMA-Hf pulses were increased from 0.05 to 0.5 s (extended) after 8 ALD cycles. A red asterisk (*) indicates the transition from the shorter to the longer TDMA-Hf pulses. The following TDMA-Hf pulses after * were 0.5 s long. Variations in intensity caused by raster scan are observed as the sample was not completely flat with respect to the analyzer and the focus shifted accordingly. Therefore, only relative intensities are comparable. Note that there are breaks between the bottom, middle, and top panels; therefore, the counting of some pulses is omitted here. We refer the reader to Figure S3 in the SI for a more complete representation of the pulse sequence.

component in O 1s are observed indicating the continuous growth of the HfO_x.

The time-resolved data reveal no clear signatures of TDMA-derived ligands in N 1s or C 1s core levels on the ACIGS surface during the initial TDMA-Hf precursor pulses. Note that the N 1s intensity is challenging to detect in the snapshot data due to its typically weak signal. A weak ligand signal is consistent with our earlier observations on low-GGI ACIGS treated with RbF,[11] suggesting that ligand retention is not a dominant feature in these systems. The absence of detectable intermediate species further supports that nucleation proceeds slowly and only becomes effective once repeated TDMA-Hf/H_2O exposures create sufficient reactive sites for film growth. Further insight into the ALD surface chemistry is expected from the detailed core level spectra recorded after selected stages during the ALD growth and discussed below.

The mass spectrometry data were recorded during the measurements to track the onset of our respective precursor

https://doi.org/10.1021/acsaem.5c03123
ACS Appl. Energy Mater. 2026, 9, 886−895

pulses using a quadrupole mass spectrometer (QMS) connected to the gas outlet line. Figure 4 illustrates part of

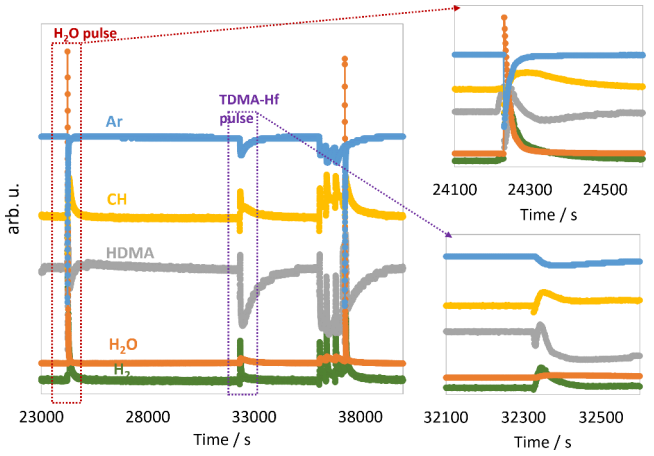

Figure 4. QMS data for HDMA (m/z = 45), Ar (m/z = 40), CH (m/z = 13), H_2O (m/z = 18), and H_2 (m/z = 2), during the initial HfO_x growth on high-GGI ACIGS recorded after 8 ALD cycles and 1 extended TDMA-Hf pulse under the following sequence: H_2O-TDMA-Hf × $4H_2O$ pulses (panels 5−7 in Figure S3). The insets illustrate a zoom-in during the H_2O (top) or TDMA-Hf (bottom) pulses.

the MS data where consecutive precursor pulses were applied. The monitored m/z values include 45 amu for HDMA, 13 amu for CH, 18 amu for H_2O, and 2 amu for H_2 during the initial HfO_x growth on high-GGI ACIGS and are recorded after 8 ALD cycles and 1 extended TDMA-Hf pulse under the following sequence: H_2O-TDMA-Hf × $4H_2O$ pulses (panels 5−7 in Figure S3). The onset of the pulses seen on QMS align well with the changes observed in the time-resolved spectra shown in Figure S3 even though the time-resolved spectra have been stopped to record the detailed core level spectra, while the QMS run continuously. The QMS data reveal signals associated with precursor delivery, as well as their fragmentation and decomposition. Specifically, HDMA may correspond to the fragmentation pattern of TDMA-Hf during the pulses, while H_2O signals are observed during water pulses. The detection of HDMA, especially immediately after each individual half-pulse, along with hydrocarbon fragments such as CH, may indicate ligand decomposition or byproduct formation, especially that HfO_x growth is observed in the XPS spectra. Additionally, the prolonged presence of H_2 signals following the H_2O and TDMA-Hf pulses likely suggests ongoing precursor decomposition and ligand removal processes.

Overall, the results indicate that surface reactions are limited at early stages of HfO_x growth and are driven by cumulative precursor exposure rather than immediate ligand retention.

3.3. Core-Level Spectra during and after HfO_x Growth

As the time-resolved measurements mainly showed that the HfO_x growth on high-GGI ACIGS proceeds after several ALD pulses and increased TDMA-Hf pulse length, we analyzed the core level spectra recorded during the purging period after selected ALD pulses (postpulse stage). The analysis focuses on comparing the relative intensities and binding energies of signals associated with the absorber surface and ALD precursors.

Figure 1 and Figure S1 in the SI show the core level spectra recorded at different stages: prior to ALD, after three TDMA-Hf pulses, after several TDMA-Hf pulses followed by 8 ALD cycles and one extended TDMA-Hf pulse, after 9 ALD cycles and one extended TDMA-Hf pulse, and after 12 ALD cycles. Note that the core level spectra were recorded following TDMA-Hf pulse(s), except for those after the 12 ALD cycles, which concluded with an H_2O pulse. Selected time-resolved spectra together with core level spectra (Rb 3d, C 1s, O 1s, and Ga 3d/In 4d/Hf 4f) recorded before, during and after the ALD growth are shown in Figure 3 e−h. All spectra were recorded under a continuous Ar flow at a pressure of approximately 1.2 mbar and a sample temperature of 180 °C, to ensure that the surface state remained stable between ALD exposure and XPS measurements.

3.4. Surface Changes after Three TDMA-Hf Pulses

The individual core level spectra in Figure 1 reveal that the surface chemistry of ACIGS is nearly unaffected by the initial TDMA-Hf pulses compared to the pre-ALD state. After three TDMA-Hf pulses, only a very weak Hf 4f signal (~17.5 eV) is observed in the Ga 3d/In 4d/Hf 4f core level spectra with a dominating Ga 3d signal, indicating that the TDMA-Hf precursor has difficulties to adsorb onto the ACIGS surface. Besides some intensity changes, no significant changes in the shape or binding energy of the absorber elements (Ga, Ag, Se) and Rb are observed during the first three ALD pulses, indicating that the chemical environment around these elements is not modified. A very weak signal appears in the N 1s spectrum following 3 TDMA-Hf pulses, which seems characteristic of dissociative or reactive adsorption of TDMA-Hf on surfaces.[23] The increase in the Ag and Rb signals may suggest some Ag diffusion toward the surface. Additionally, the In 3d spectra begin to exhibit a new component at higher binding energy, shifted to higher binding energy by +0.6 eV, suggesting the presence of additional In species. A likely explanation for this shift is the formation of In−O compounds, such as In_2O_3, as the observed binding energy is close to reported values for In−O (~445.5 eV). This is in contrast to a previous study, where TDMA-Hf pulses were shown to remove In_2O_3 from InAs.[9,10] The formation of this oxide species during the initial TDMA-Hf pulse implies that oxygen is already present at or near the surface, likely due to residual surface oxygen or oxygen diffusing from below the surface. Additionally, In diffusion to the surface may contribute to local In enrichment, enabling the formation of In−O bonds during the early stages of ALD. While a native In-oxide may pre-exist, the oxide species forming during the Hf precursor exposure could differ in structure or stoichiometry,[24] possibly influenced by interactions with TDMA-Hf[9] or partial ligand exchange. Alternatively, we may also consider the formation of mixed anion phases such as (Ag,Rb)−In−(Se,O), particularly in the chemically complex surface environment following RbF treatment and under ALD conditions, as previously observed[5] in chalcopyrite absorbers.

The main difference observed between the low-GGI[11] and high-GGI (present study) ACIGS samples during the initial TDMA-Hf pulses is the significantly slower HfO_x growth in the high-GGI ACIGS sample. While HfO_x formation is evident after just a few TDMA-Hf pulses (identical pulses as in the present study) in the low-GGI ACIGS sample treated with RbF, little to no HfO_x is detected in the high-GGI sample under comparable conditions. This is clearly visible by

https://doi.org/10.1021/acsaem.5c03123
ACS Appl. Energy Mater. 2026, 9, 886−895

comparing the Hf 4f/In 4d/Ga 3d core level spectra for both the low- and high-GGI ACIGS samples after 3 TDMA-Hf pulses (Figure S4 in the SI). A likely explanation is the formation of a thicker alkali-metal-containing surface layer on the high-GGI sample following RbF treatment, which may inhibit TDMA-Hf adsorption and nucleation and subsequent surface reactions by blocking reactive sites. In addition, the diffusion of Rb toward the surface during precursor exposure may cause a slower HfO_x growth, as these alkali species can dominate the surface signal and obscure the initial oxide formation. Thus, the results suggest that the surface compositional differences prior to ALD between the low- and high-GGI ACIGS samples (Cu-depleted and Se- and alkali-enriched surface for high-GGI ACIGS) have a significant impact on subsequent ALD growth by altering precursor adsorption dynamics and potentially influencing the chemical reactivity at the ACIGS/oxide interface.

3.5. Surface Changes after Several TDMA-Hf Pulses, Eight ALD Cycles, and One Extended TDMA-Hf Pulse

Since no HfO_x growth was observed after three TDMA-Hf pulses (0.05 s each), the sample was subsequently exposed to 8 additional ALD cycles (alternating TDMA-Hf and H_2O pulses, 0.05 s each) and finally to a longer TDMA-Hf pulse (0.5 s), denoted as 8 ALD + TDMA-Hf in Figures 1 and 3. The onset of HfO_x growth became evident after such sequence, indicated by a pronounced decrease in the substrate core level signals (Ag 3d, In 3d, Ga 2p, Se 3d) and a corresponding increase in the O 1s component associated with Me−O_x species and Hf 4f signal (~17.0 eV), suggesting the growth of HfO_x during the TDMA-Hf exposure. The Me−OH component in O 1s is also increasing, likely as a result of surface hydroxylation during the water pulses. This is also evident by the position of the maximum intensity of the Hf 4f line after the repeated TDMA-Hf pulses and ALD cycles, appearing at ~17.0 eV—slightly lower than the binding energy typically reported for HfO_2 (17.6 eV[9,25])—suggesting a mixture of Hf−O and Hf−OH bonding environments. The continued presence of substrate peaks suggests that the HfO_x film at this stage remains very thin (roughly 2 nm) or incomplete (with openings). Further, aside from minor intensity variations, no significant changes in the shape or binding energy of the Ag, In, and Se core-level spectra were observed (within the energy resolution of the experiments of 0.5 eV) during HfO_x growth, indicating that their chemical environments remain largely unchanged. However, some changes are observed in the Ga 3d signal. Notably, the Ga 3d/In 4d/Hf 4f core-level spectra reveal a new Ga-related component at higher binding energy (+0.8 eV relative to the main Ga peak), labeled as Ga II (pink), which likely corresponds to the formation of Ga−F or Ga−O species.[17,24,26] This suggests the formation of Ga−F bonds by the reaction of fluorides with GaO_3.[27] Such bonding environments are known to shift the Ga 3d peak to higher binding energies compared to Ga−Se bonds in the chalcopyrite lattice. The new component is not clearly resolved in the Ga 2p spectrum, which probes only the near-surface region (probing depth at employed photon energy ~2 nm) and is therefore less sensitive to subsurface chemical states. The Ga 3d peak, with its larger probing depth (~4.5 nm), is more likely to capture contributions from Ga−F species located below the immediate surface. This explains why signatures of Ga−F (or Ga−O) bonding are more evident in the Ga 3d region.

Besides the very weak signal observed in the N 1s spectrum during the HfOx growth, the presence of organic ligands on the surface is not clearly visible in the C 1s core level, suggesting either that they are removed during the purge period following a TDMA-Hf pulse or are removed during the water pulse. A weak C 1s component at ~285.6 eV (blue − C II) emerged, likely due to formation of C−O(H) and HCOO. This observation deviates from standard ALD models.[28] While the water pulse is expected to remove organic ligands and replace them with OH^- groups, the unclear presence of ligands before the water step suggests that additional surface reactions or unexpected ligand removal mechanisms may be occurring.[29,30]

The spectra recorded after several TDMA-Hf pulses + 8 ALD cycles + an extended TDMA-Hf pulse show the presence of a second Rb 3d doublet (blue, Rb II) shifted about 0.8 eV to higher BE and assigned to RbF, as was previously observed during HfO_x growth on low-GGI ACIGS. This finding aligns with the observed increase in fluorine species, supporting the idea of fluorine diffusion and RbF formation during ALD. In our previous study on low-GGI ACIGS,[11] Rb species have been shown to diffuse toward the surface and form new phases (Rb−In−Se, Rb−F), thereby influencing the initial stages of ALD growth. It is likely that similar species, but in different amounts, develop under the HfO_x growth on high-GGI ACIGS in this case. These findings suggest a complex surface evolution in which alkali-metal-containing phases persist, while nucleation becomes possible due to local chemical activation.

3.6. After Several TDMA-Hf Pulses and 9 ALD Cycles

Once the HfO_x growth started, another H_2O (0.05 s) pulse (forming another complete ALD cycle with TDMA-Hf) and one more extended TDMA-Hf (0.5 s) pulse were carried out (denoted as 9 ALD cycles + TDMA-Hf in Figure 1). Aside from intensity variations, the core level spectra show no changes indicative of new chemical environments. The intensity of hydroxyl species increased compared to 8 ALD cycles + TDMA-Hf pulse, as indicated by the O II component in the O 1s core level spectra. In contrast, the component in the C 1s spectrum at higher binding energy (blue, C II) has not changed during the H_2O pulse. This is likely due to these species being C−O(H) and HCOO, which are not readily removed by water. A decrease of absorber signals and increase in the Hf 4f signal is observed, indicating HfO_x growth. Further, an increase in the Na, Rb, and F signals is observed, most likely due to increased surface concentration due to diffusion. These results suggest that the evolving species are more appropriately described as alkali-metal-containing secondary phases since Na diffusion is more significant in the high-GGI sample during HfO_x growth. This is likely due to more Rb diffusing toward the surface, a behavior known for alkali metals under heat and reactive conditions, and also shown in our earlier work.[11] Notably, the Rb I component in Rb 3d alkali ((Alk)-In-Se) appears to increase more prominently during HfO_x growth, compared to Rb−F species (blue − Rb II). This is somewhat unexpected, given that the alkali-metal-containing layer is assumed to block precursor adsorption in the initial stages by passivating the surface. One possible explanation is that the ALD process—particularly the H_2O pulses—may alter the chemical environment at the surface, enabling the redistribution or even partial reformation of alkali-metal-containing species as surface reactions proceed. Alternatively, rather than acting solely as a passive barrier, the alkali-metal-

https://doi.org/10.1021/acsaem.5c03123
ACS Appl. Energy Mater. 2026, 9, 886−895

containing phase may behave dynamically under ALD conditions, coexisting with −OH groups that are required to activate the TDMA-Hf precursor. This suggests that the role of Rb-containing species may be more complex than initially assumed, potentially contributing to both inhibition and facilitation of film growth at different stages.

3.7. After Several TDMA-Hf Pulses and 12 ALD Cycles

Notably, several TDMA-Hf pulses and 12 full ALD cycles were required to observe the formation of a thicker HfO_x layer, as indicated by significantly reduced substrate signals (top spectra in Figures 1 and 3). The core level intensities of the ACIGS absorber decreased significantly, while the Hf 4f core level signal increased, suggesting improved surface coverage. A decrease in both carbon intensity and the extra Ga component intensity was observed due to increased HfO_x coverage.

A comparison of the (Na+Rb)/(Ag+Cu) surface composition ratio before and after HfO_x ALD on the high-GGI ACIGS sample reveals a pronounced alkali accumulation, with the ratio increasing nearly 6-fold from 16 to 94. In addition, the Rb/(In +Ga) surface ratio also shows a significant increase from 0.1 to 1.8, while the Se/(Ag+Cu+In+Ga) ratio increased 3-fold from 4 to 11.6. The GGI ratio decreased from 0.66 to 0.60 after HfO_x ALD, whereas the bulk GGI ratio for high-Ga-content ACIGS was measured to be 0.82. This change is likely due to preferential surface depletion of Ga during growth, as well as possible surface segregation induced by the ALD process.[31,32]

3.8. Comparison of Low- and High-GGI ACIGS (+RbF PDT) Absorbers in HfO_xALD Growth

The ALD behavior on ACIGS absorbers can strongly be influenced by the absorber composition and postdeposition treatments, which affects both the band gap and the surface properties of the material. Higher GGI ratios not only widen the band gap but also alter surface composition and reduce the density of reactive sites for precursor adsorption, which may further be enhanced by a RbF treatment. These changes may significantly impact nucleation dynamics and interface formation during the early stages of ALD, necessitating composition-specific process optimization. In our previous study,[11] we investigated the surface chemistry of RbF-treated, low-GGI ACIGS (GGI = 0.4) during the very first ALD cycle of HfO_x, revealing that alkali-induced surface modification slows down precursor adsorption as compared to a sample without a RbF PDT. Despite the slower initial growth, the results indicate that HfO_x still forms after a few TDMA-Hf pulses and nearly completely covers the ACIGS surface after a full ALD cycle that consisted of several TDMA-Hf pulses and one water pulse. The study was limited to a single ALD cycle and a single absorber composition.

To expand on these findings and in an attempt to grow a thicker HfO_x, the low- and high-GGI ACIGS samples with RbF-PDT (GGI ratios of 0.4 and 0.8, respectively) were subjected to several HfO_x ALD sequences (TDMA-Hf and H_2O pulses) until surface saturation was reached, as indicated by the significant decrease in the absorber core-level signals compared to before ALD. The data for high-GGI ACIGS is presented in Figure 1, while the corresponding results for low-GGI sample are shown in Figure S5 in the SI. Even though the XPS spectra were decomposed using the same parameters as in our previous study on a low-GGI absorber (Figure S4 in ref 11), a single component for Hf 4f was needed to obtain a satisfactory fit for the thicker HfO_x shown in Figure S5 in the SI, thus indicating that the Hf−F or Hf−O−F species previously observed during the initial stages of growth may only be present at the interface to the ACIGS but are not observed on a thicker film.

A comparison of the low- and high-GGI ACIGS samples shows that there are some differences in surface composition and reactivity, likely influencing ALD nucleation behavior and the formation of interfacial layers. As discussed above, for the high-GGI ACIGS, a Cu-depleted, and Se, alkali enriched surface is observed, leading to the formation of alkali-metal containing phases after RbF postdeposition treatment prior to ALD. This layer likely blocks available surface sites for TDMA-Hf adsorption and reaction, as evidenced by the negligible Hf signal even after several TDMA-Hf pulses. As a result, HfO_x growth is significantly delayed, and no HfO_x is observed after the initial TDMA-Hf pulses. The ALD growth only begins after several additional TDMA-Hf and H_2O pulses as well as increased TDMA-Hf pulse lengths. HfO_x growth is not observed on the high-GGI ACIGS sample before water pulses. Water exposure plays a crucial role by introducing surface hydroxyl groups that enable TDMA-Hf adsorption and oxide nucleation, rather than removing the alkali-metal-containing layer. Thus, H_2O chemically activates the surface for HfO_x growth through hydroxylation, not by dissolving or thinning the existing passivation layer. Consequently, oxide nucleation proceeds more readily on the low-GGI sample with its more accessible surface sites, whereas the high-GGI sample remains hindered.

For the high-GGI sample, the formation of Ga−F and In−O species is evident, features that were not previously observed in the low-GGI ACIGS (Figure 5). The In−O species present in the In 3d spectrum of the high-GGI ACIGS suggests the formation of a chemically distinct In environment at the surface, emerging right after the initial TDMA-Hf pulses. Such features are absent in the low-GGI sample, where only single, well-defined doublets are observed, pointing to a more uniform and chemically stable surface. One possible explanation is that the higher Ga content in high-GGI (GGI) ACIGS leads to subtle alterations in surface reconstruction or phase separation, promoting the formation of In-rich domains that are more oxidized or structurally distinct.

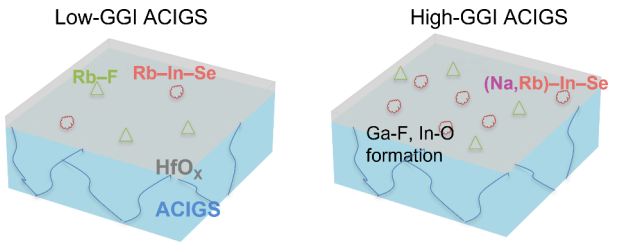

Figure 5. Schematic representation comparing the HfO_x ALD growth on low-GGI and high-GGI ACIGS samples after several ALD cycles

Further, reduced oxygen diffusion is observed during the TDMA-Hf pulses on high-GGI ACIGS, likely due to the thicker layer blocking oxygen transport and hindering HfO_x formation. These observations indicate that the ACIGS GGI ratio influences not only nucleation dynamics but also the dominant surface reaction pathways during the early stages of ALD. Thus, both pulse length but also the order of ALD pulse (water or metal precursor) seem to play an important role in the ALD growth of HfO_x on ACIGS.

https://doi.org/10.1021/acsaem.5c03123
ACS Appl. Energy Mater. 2026, 9, 886−895

4. CONCLUSIONS

This study demonstrates that the ALD nucleation of HfO_x on RbF-treated ACIGS absorbers is strongly governed by bulk composition and surface chemistry. *In situ* AP-XPS reveals that high-GGI ACIGS exhibits a Cu-depleted, Se- and Rb-enriched surface dominated by an alkali-metal-containing phase (likely some (Na,Rb)−In−(Se,O) agglomerates) prior to HfO_x growth, which suppresses precursor adsorption and significantly delays HfO_x growth compared to low-GGI absorbers. Water pulses are shown to be essential for activating these surfaces through hydroxylation, thereby enabling TDMA-Hf activation and subsequent oxide formation. Moreover, the emergence of Ga−F and In−O species as well as Na diffusion exclusively in high-GGI ACIGS highlights the composition-dependent chemical pathways that influence nucleation dynamics. These findings establish that absorber composition and alkali postdeposition treatments critically determine the uniformity of ALD passivation layers in ACIGS solar cells.

■ ASSOCIATED CONTENT

Supporting Information

The Supporting Information is available free of charge at https://pubs.acs.org/doi/10.1021/acsaem.5c03123.

Binding energy positions (eV) for high-GGI and low-GGI ACIGS samples during ALD, *in situ* time-resolved AP-XPS measurements, Se 3d normalized data, and Hf 4f/In 4d/Ga 3d core-level spectra recorded for both low- and high-GGI ACIGS (PDF)

■ AUTHOR INFORMATION

Corresponding Authors

Melike Babucci − *Solar Cell Technology, Department of Materials Science and Engineering, Uppsala University, SE-751 21 Uppsala, Sweden;* orcid.org/0000-0001-7785-3755; Email: melike.babucci@angstrom.uu.se

Natalia M. Martin − *Solar Cell Technology, Department of Materials Science and Engineering, Uppsala University, SE-751 21 Uppsala, Sweden;* orcid.org/0000-0002-6881-4989; Email: natalia.martin@angstrom.uu.se

Authors

Lars Stolt − *Solar Cell Technology, Department of Materials Science and Engineering, Uppsala University, SE-751 21 Uppsala, Sweden*

Esko Kokkonen − *MAX IV Laboratory, Lund University, SE-221 00 Lund, Sweden;* orcid.org/0000-0002-3674-7486

Rainer Timm − *Division of Synchrotron Radiation Research, Department of Physics, Lund University, SE-221 00 Lund, Sweden;* orcid.org/0000-0001-8914-5924

Joachim Schnadt − *Division of Synchrotron Radiation Research, Department of Physics and MAX IV Laboratory, Lund University, SE-221 00 Lund, Sweden;* orcid.org/0000-0001-9375-831X

Charlotte Platzer-Björkman − *Solar Cell Technology, Department of Materials Science and Engineering, Uppsala University, SE-751 21 Uppsala, Sweden;* orcid.org/0000-0002-6554-9673

Tobias Törndahl − *Solar Cell Technology, Department of Materials Science and Engineering, Uppsala University, SE-751 21 Uppsala, Sweden;* orcid.org/0000-0001-7757-5847

Complete contact information is available at: https://pubs.acs.org/10.1021/acsaem.5c03123

Notes

The authors declare no competing financial interest.

■ ACKNOWLEDGMENTS

This work was financially supported by the Swedish Research Council (grant nos. 2020-04065, 2021-5627, and 2023-03492), the Swedish Energy Agency (grant no. 48479-1), and the StandUp for Energy programme. We acknowledge the MAX IV Laboratory for time on the SPECIES beamline under proposal no. 20221137. Research conducted at MAX IV, a Swedish national user facility, is supported by the Vetenskapsrådet (Swedish Research Council, VR) under contract 2018-07152, VINNOVA (Swedish Governmental Agency for Innovation Systems) under contract 2018-04969, and Formas under contract 2019-02496.

■ REFERENCES

(1) Edoff, M.; Jarmar, T.; Nilsson, N. S.; Wallin, E.; Högström, D.; Stolt, O.; Lundberg, O.; Shafarman, W.; Stolt, L. High Voc in (Cu,Ag)(In,Ga)Se_2 Solar Cells. *IEEE J. Photovolt* **2017**, *7* (6), 1789−1794.

(2) Keller, J.; Kiselman, K.; Donzel-Gargand, O.; Martin, N. M.; Babucci, M.; Lundberg, O.; Wallin, E.; Stolt, L.; Edoff, M. High-Concentration Silver Alloying and Steep Back-Contact Gallium Grading Enabling Copper Indium Gallium Selenide Solar Cell with 23.6% Efficiency. *Nat. Energy.* **2024**, *9*, 467−478.

(3) Chirilă, A.; Reinhard, P.; Pianezzi, F.; Bloesch, P.; Uhl, A. R.; Fella, C.; Kranz, L.; Keller, D.; Gretener, C.; Hagendorfer, H.; Jaeger, D.; Erni, R.; Nishiwaki, S.; Buecheler, S.; Tiwari, A. N. Potassium-Induced Surface Modification of Cu(In,Ga)Se_2 Thin Films for High-Efficiency Solar Cells. *Nat. Mater.* **2013**, *12* (12), 1107−1111.

(4) Bombsch, J.; Avancini, E.; Carron, R.; Handick, E.; Garcia-Diez, R.; Hartmann, C.; Félix, R.; Ueda, S.; Wilks, R. G.; Bär, M. NaF/RbF-Treated Cu(In,Ga)Se_2 Thin-Film Solar Cell Absorbers: Distinct Surface Modifications Caused by Two Different Types of Rubidium Chemistry. *ACS Appl. Mater. Interfaces* **2020**, *12* (31), 34941−34948.

(5) Donzel-Gargand, O.; Larsson, F.; Törndahl, T.; Stolt, L.; Edoff, M. Secondary Phase Formation and Surface Modification from a High Dose KF-Post Deposition Treatment of (Ag,Cu)(In,Ga)Se_2 Solar Cell Absorbers. *Prog. Photovolt. Res. Appl.* **2019**, *27* (3), 220−228.

(6) Jackson, P.; Wuerz, R.; Hariskos, D.; Lotter, E.; Witte, W.; Powalla, M. Effects of Heavy Alkali Elements in Cu(In,Ga)Se_2 Solar Cells with Efficiencies up to 22.6%. *Phys. Status Solidi-Rapid Res. Lett.* **2016**, *10* (8), 583−586.

(7) Birant, G.; Mafalda, J.; Scaffidi, R.; de Wild, J.; Buldu, D. G.; Kohl, T.; Brammertz, G.; Meuris, M.; Poortmans, J.; Vermang, B. Rear Surface Passivation of Ultra-Thin CIGS Solar Cells Using Atomic Layer Deposited HfOx. *EPJ. Photovolt.* **2020**, *11*, 10.

(8) Löckinger, J.; Nishiwaki, S.; Bissig, B.; Degutis, G.; Romanyuk, Y. E.; Buecheler, S.; Tiwari, A. N. The Use of HfO_2 in a Point Contact Concept for Front Interface Passivation of Cu(In,Ga)Se_2 Solar Cells. *Sol. Energy Mater. Sol. Cells* **2019**, *195*, 213−219.

(9) D'Acunto, G.; Troian, A.; Kokkonen, E.; Rehman, F.; Liu, Y.-P.; Yngman, S.; Yong, Z.; McKibbin, S. R.; Gallo, T.; Lind, E.; Schnadt, J.; Timm, R. Atomic Layer Deposition of Hafnium Oxide on InAs: Insight from Time-Resolved in Situ Studies. *ACS Appl. Electron. Mater.* **2020**, *2* (12), 3915−3922.

(10) D'Acunto, G.; Shayesteh, P.; Kokkonen, E.; Boix de la Cruz, V.; Rehman, F.; Mosahebfard, Z.; Lind, E.; Schnadt, J.; Timm, R. Time Evolution of Surface Species during the ALD of High-k Oxide on InAs. *Surf. Interfaces* **2023**, *39*, No. 102927.

(11) Martin, N. M.; Babucci, M.; Stolt, L.; Hultqvist, A.; Kokkonen, E.; Timm, R.; Schnadt, J.; Platzer-Björkman, C.; Törndahl, T. Situ Studies of Atomic Layer Deposition of Hafnium Oxide on (Ag,Cu)

In,Ga)Se_2 for Thin Film Solar Cells. *ACS Appl. Energy Mater.* **2025**, *8*, 461−472.
(12) Scofield, J. H. *Theoretical Photoionization Cross Sections from 1 to 1500 keV; UCRL--51326*; Lawrence Livermore National Laboratory: Livermore, CA, USA, 1972.
(13) Tanuma, S.; Powell, C. J.; Penn, D. R. Calculations of Electron Inelastic Mean Free Paths. V. Data for 14 Organic Compounds over the 50−2000 eV Range. *Surf. Interface Anal.* **1994**, *21* (3), 165−176.
(14) QUASES-IMFP-TPP2M - QUASES. Available online http://www.quases.com/products/quases-imfp-tpp2m/.
(15) IGOR Pro Software. Wavemetrics. Available online https://www.wavemetrics.com/node/21549.
(16) Kreikemeyer-Lorenzo, D.; Hauschild, D.; Jackson, P.; Friedlmeier, T. M.; Hariskos, D.; Blum, M.; Yang, W.; Reinert, F.; Powalla, M.; Heske, C.; Weinhardt, L. Rubidium Fluoride Post-Deposition Treatment: Impact on the Chemical Structure of the Cu(In,Ga)Se_2 Surface and CdS/Cu(In,Ga)Se_2 Interface in Thin-Film Solar Cells. *ACS Appl. Mater. Interfaces* **2018**, *10* (43), 37602−37608.
(17) Maticiuc, N.; Kodalle, T.; Lauche, J.; Wenisch, R.; Bertram, T.; Kaufmann, C. A.; Lauermann, I. In Vacuo XPS Investigation of Cu(In,Ga)Se_2 Surface after RbF Post-Deposition Treatment. *Thin Solid Films* **2018**, *665*, 143−147.
(18) Boumenou, M.; et al. Nanoscale Surface Analysis Reveals Origins of Enhanced Interface Passivation in RbF Post Deposition Treated CIGSe Solar Cells. *Adv. Funct. Mater.* **2023**, *33* (30), No. 2300590.
(19) Avancini, E.; Carron, R.; Weiss, T. P.; Andres, C.; Bürki, M.; Schreiner, C.; Figi, R.; Romanyuk, Y. E.; Buecheler, S.; Tiwari, A. N. Effects of Rubidium Fluoride and Potassium Fluoride Postdeposition Treatments on Cu(In,Ga)Se_2 Thin Films and Solar Cell Performance. *Chem. Mater.* **2017**, *29* (22), 9695−9704.
(20) Martin, N. M.; Törndahl, T.; Wallin, E.; Simonov, K. A.; Rensmo, H.; Platzer-Björkman, C. Surface/Interface Effects by Alkali Postdeposition Treatments of (Ag,Cu)(In,Ga)Se_2 Thin Film Solar Cells. *ACS Appl. Energy Mater.* **2022**, *5* (1), 461−468.
(21) Keller, J.; Aboulfadl, H.; Stolt, L.; Donzel-Gargand, O.; Edoff, M. Rubidium Fluoride Absorber Treatment for Wide-Gap (Ag,Cu)-(In,Ga)Se_2 Solar Cells. *Sol. RRL* **2022**, *6* (6), No. 2200044.
(22) Maticiuc, N.; Kodalle, T.; Ümsür, B.; Bertram, T.; Wenisch, R.; Wang, Y.; Majumdar, I.; Yetkin, H. A.; Abou-Ras, D.; Schäfer, N.; Kaufmann, C. A.; Schlatmann, R.; Lauermann, I. Depth-Resolved Analysis of the Effect of RbF Post Deposition Treatment on CIGSe with Two Different Cu Concentrations. *Sol. Energy Mater. Sol. Cells* **2021**, *226*, No. 111071.
(23) Head, A.; Chaudhary, S.; Olivieri, G.; Bournel, F.; Andersen, J. N.; Rochet, F.; Gallet, J.-J.; Schnadt, J. Near Ambient Pressure X-Ray Photoelectron Spectroscopy Study of the Atomic Layer Deposition of TiO_2 on RuO_2(110). *J. Phys. Chem. C* **2016**, *120* (1), 243−251.
(24) Pyatenko, E.; Hauschild, D.; Mikhnych, V.; Edla, R.; Steininger, R.; Hariskos, D.; Witte, W.; Powalla, M.; Heske, C.; Weinhardt, L. Rb Diffusion and Oxide Removal at the RbF-Treated Ga_2O_3/Cu(In,Ga)-Se_2 Interface in Thin-Film Solar Cells. *ACS Appl. Mater. Interfaces* **2023**, *15*, 53113−53121.
(25) Lee, J.-C.; Oh, S.-J.; Cho, M.; Hwang, C. S.; Jung, R. Chemical Structure of the Interface in Ultrathin HfO_2/Si Films. *Appl. Phys. Lett.* **2004**, *84* (8), 1305−1307.
(26) Valdes, N. H.; Jones, K. J.; Opila, R. L.; Shafarman, W. N. Influence of Ga and Ag on the KF Treatment Chemistry for CIGS Solar Cells. *IEEE J. Photovolt.* **2019**, *9* (6), 1846−1851.
(27) Barrière, A. S.; Couturier, G.; Gevers, G.; Guégan, H.; Seguelond, T.; Thabti, A.; Bertault, D. Preparation and Characterization of Gallium(III) Fluoride Thin Films. *Thin Solid Films* **1989**, *173* (2), 243−252.
(28) Methaapanon, R.; Bent, S. F. Comparative Study of Titanium Dioxide Atomic Layer Deposition on Silicon Dioxide and Hydrogen-Terminated Silicon. *J. Phys. Chem. C* **2010**, *114* (23), 10498−10504.
(29) Parsons, G. N.; Atanasov, S. E.; Dandley, E. C.; Devine, C. K.; Gong, B.; Jur, J. S.; Lee, K.; Oldham, C. J.; Peng, Q.; Spagnola, J. C.; Williams, P. S. Mechanisms and Reactions during Atomic Layer Deposition on Polymers. *Coord. Chem. Rev.* **2013**, *257* (23), 3323−3331.
(30) Parsons, G. N.; George, S. M.; Knez, M. Progress and Future Directions for Atomic Layer Deposition and ALD-Based Chemistry. *MRS Bull.* **2011**, *36* (11), 865−871.
(31) Babucci, M.; Meira, D. M.; Wallin, E.; Keller, J.; Donzel-Gargand, O.; Platzer-Björkman, C.; Martin, N. M. Depth-Dependent Atomic-Scale Structural Changes in (Ag,Cu)(In,Ga)Se_2 Absorbers Relevant for Thin-Film Solar Cells. *ACS Appl. Energy Mater.* **2023**, *6* (18), 9264−9275.
(32) Aboulfadl, H.; Sopiha, K. V.; Keller, J.; Larsen, J. K.; Scragg, J. J. S.; Persson, C.; Thuvander, M.; Edoff, M. Alkali Dispersion in (Ag,Cu)(In,Ga)Se_2 Thin Film Solar Cells—Insight from Theory and Experiment. *ACS Appl. Mater. Interfaces* **2021**, *13* (6), 7188−7199.

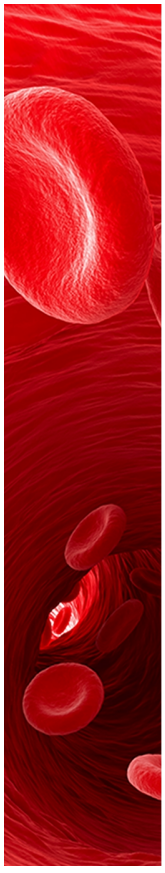
CAS BIOFINDER DISCOVERY PLATFORM™
CAS BIOFINDER HELPS YOU FIND YOUR NEXT BREAKTHROUGH FASTER
Navigate pathways, targets, and diseases with precision
Explore CAS BioFinder
CAS
A division of the American Chemical Society

https://doi.org/10.1021/acsaem.5c03123
ACS Appl. Energy Mater. 2026, 9, 886−895